



Stefan Madlmeir, BSc

DEM simulation of the dosator process for capsule filling

MASTER'S THESIS

to achieve the university degree of

Diplom-Ingenieur

Master's degree programme: Chemical and Process Engineering

submitted to

Graz University of Technology

Supervisor

Univ.-Prof. Dipl.-Ing. Dr. techn. Johannes Khinast
Institute of Process and Particle Engineering

Co-Supervisor

Dipl.-Ing. Dipl.-Ing Peter Loidolt, BSc
Institute of Process and Particle Engineering

Graz, April 2018

Affidavit

I declare that I have authored this thesis independently, that I have not used other than the declared sources/resources, and that I have explicitly indicated all material which has been quoted either literally or by content from the sources used. The text document uploaded to TUGRAZonline is identical to the present master's thesis.

Date

Signature

Abstract

Hard gelatin capsules are besides tablets a commonly used solid oral dosage form. An industrially used method for capsule filling is the dosator process. The fill weight and the fill weight variability as the main quality attributes are difficult to control, since the dosator process is a volume based approach. Therefore excellent process understanding is necessary. With the help of DEM simulations the impact of critical parameters on the filling behavior is investigated. For this purpose two different contact models are verified, calibrated and validated. Contrary to the Hertz model, the results of the Luding model turned out to be satisfactory. The examined process parameters include the machine speed, powder bed height, gap width, dosator geometry and bulk density variations. It is shown that no volumetric filling occurs and a homogeneous bed is necessary in order to reduce fill weight variations.

Kurzfassung

Zur oralen Einnahme von Medikamenten werden neben Tabletten auch häufig Gelatinekapseln verwendet. Diese werden mittels des sogenannten Dosatorprozesses befüllt. Sowohl die durchschnittliche Masse als auch deren Variabilität sind wichtige Qualitätskriterien. Diese sind jedoch schwer kontrollierbar, da der Füllprozess auf einem konstanten Volumen des Dosators basiert. Daher ist ein ausgeprägtes Prozessverständnis unumgänglich, um hohe Qualitäten zu erreichen. Mittels DEM-Simulationen werden wichtige Prozessparameter und ihre Auswirkungen auf die Füllmenge untersucht. Dafür wurden zwei Kontaktmodelle auf ihre Eignung zur Reproduktion des Prozesses getestet. Während sich das Hertz-Modell als unzureichend genau herausstellt, werden mit dem Luding-Modell angemessene Resultate erzielt. Als Prozessparameter wurden unterschiedliche Füllgeschwindigkeiten, Pulverbetthöhen, Einstehtiefen, Dosatorgeometrien und Pulverbettdichten verwendet. Die Ergebnisse zeigen, dass keine volumetrische Füllung erzielt wird und dass ein homogenes Pulverbett für geringe Massenunterschiede notwendig ist.

Acknowledgment

I'd like to thank Univ.-Prof. Johannes Khinast for the possibility to write my thesis at the Institute of Process and Particle Engineering in a fascinating field of research. Special regards belong to Dipl.-Ing. Dipl.-Ing. Peter Loidolt, who was a great help when smaller or bigger problems during research occurred. Thank you for the excellent support during my time at the institute. Thanks to Peter, Andreas B., Daniela and Andreas K. as members of the Loony Science Group for countless funny moments, but also for many constructive scientific discussions. Furthermore I'd like to thank the involved members of MG2 and RCPE for the good cooperation.

Special thanks go to my girlfriend Miriam and my family who supported me in many ways during my studies.

Table of Contents

1	Introduction.....	1
2	Methods	5
2.1	DEM	5
2.2	Hertz contact model	6
2.3	Luding contact model	7
2.4	Simulation setup.....	9
2.4.1	Geometric setup.....	9
2.4.2	Dosator movement	10
3	Verification, calibration and validation	12
3.1	Verification	12
3.1.1	Hertz normal model	13
3.1.2	Hertz tangential model.....	14
3.1.3	Luding normal model	15
3.1.4	Luding tangential model.....	16
3.2	Calibration of model parameters	17
3.2.1	Fundamentals of model calibration	17
3.2.2	Design of Experiments.....	18
3.2.3	Applied calibration procedure	19
3.3	Validation.....	22
4	Results	25
4.1	Machine speed	25
4.2	Powder bed height	26
4.3	Gap width	27
4.4	Dosator geometry.....	28
4.4.1	Dosator diameter	28
4.4.2	Chamber length.....	29
4.4.3	Constant precompression ratio.....	30

4.4.4	Constant diameter to chamber length ratio	31
4.4.5	Constant dosator volume	31
4.5	Bulk density	32
5	Conclusion and outlook.....	34
6	Nomenclature.....	36
7	List of tables	37
8	List of figures	38
9	References.....	40

1 Introduction

Solid oral dosage forms are most commonly used in pharmaceutical industry, since they are convenient for the patient and come along with cost effective development (Sastry et al., 2000). In addition to tablets, hard-shell capsules are a frequently utilized dosage form for powders. Capsule shells are usually made of gelatin and consist of two parts, the body and the cap. After the filling of the body, both parts are put together. While dry powder is often used for filling, many other forms are also possible, including semisolids, liquids, mini tablets or mini capsules. Given that different fill weights are necessary for every respective drug and considering the variable bulk density of the particular powder, the volume which has to be filled into the capsules varies. Therefore different capsule sizes exist, ranging from 5 (0.13 ml) to 000 (1.36 ml). For transferring the powder into the capsule, several ways are possible. They can be divided into direct and indirect methods. Direct methods, e.g. weighing in the API, are only applicable if a small quantity of the drug is needed. Industrial production is most often done by faster indirect filling. In this case a stable plug is formed by compressing the powder. This is most commonly done by dosator systems or tamping systems. In addition to the high quantities, which can be produced with automatic systems (150,000+ capsules/hour), those methods compact the powder and therefore the volume decreases. Smaller capsules can be used, which leads to better patient convenience, since they are easier to swallow (Hoag, 2016).

Dosator systems consist of a rotating powder bed with a defined height and a dosator nozzle. The dosator nozzle is a hollow cylinder with a moving piston inside. The dosing takes place in five consecutive steps (Fig. 1):

1. The dosator dips into the powder bed until a predefined distance to the container bottom is reached. In this stage, the powder inside the dosator is precompressed. The ratio of the powder bed height and the length of the dosator chamber is known as the precompression ratio.
2. In the second stage, the piston inside the nozzle is moved down in order to compress the powder until a stable plug is formed. This step can be omitted, if the precompression of the first step provides sufficient plug stability. (Tan and Newton, 1990a) give an estimation of the necessary compression stress.
3. Afterwards the dosator is pulled out of the bed, containing the powder plug.
4. The dosator moves out of the container to the top of an empty capsule body.
5. In the last step the powder is discharged via the piston into the capsule and the cap is put on the body. The dosator nozzle shifts back to the starting position.

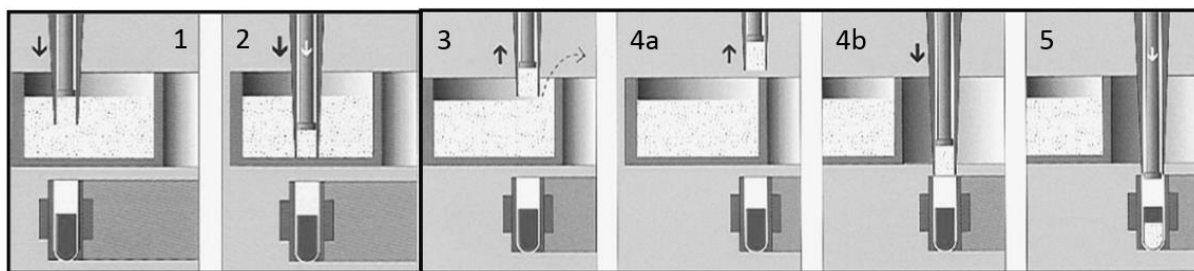


Fig. 1: Principle of the capsule filling process via the dosator method (Hoag, 2016).

A more detailed process description is provided by (Jones, 2001; Small and Augsburger, 1977). Tamping systems are not considered in this work, but explanations on how they work are stated in (Jones, 2001; Shah et al., 1983).

Due to the strict regulations in pharmaceutical industry, product uniformity is crucial. Regarding the dosator process, the capsule fill weight and the fill weight variability are the critical quality attributes (CQA). The relationships between critical process parameters (CPP) as well as critical material attributes (CMA) and the CQAs were studied extensively (Faulhammer et al., 2014a, 2014b; Jolliffe and Newton, 1982; Llusà et al., 2014, 2013; Patel and Podczeczek, 1996; Stranzinger et al., 2017; Tan and Newton, 1990b). Evidently, the capsule filling performance is highly dependent on both CPPs and CMAs. Obviously the precompression ratio (and thus the powder bed height and the dosator chamber length) and the compression ratio are important process parameters, but also the dosator geometry and the dipping speed are of relevance. In terms of material attributes, the main factors are the flowability and the compressibility of the powder. Therefore parameters as Hausner's ratio, angle of repose, Jenike's flow factor, Carr's compressibility and of course the particle size and shape are relevant CMAs. Particularly for low-dose systems with small dosator diameters also the wall friction angle shows substantial influence on the fill weight. Another important requirement for low fill weight variabilities is a constant bulk density of the powder bed. A constant bulk density is difficult to obtain though, since it is affected by processing history, machine vibrations, humidity and several other hardly manageable factors. Furthermore the powder bed in the container is not necessarily homogenous, especially if cohesive materials are used.

Since the dosator process is highly dependent on many CPPs and CMAs, getting full process understanding out of experiments is hardly possible. Modeling and simulation can support experiments to improve process understanding. In general, simulations are able to determine process variables, which can't be measured in experiments, e.g. the evolution of the mass inside the dosator during the dipping step. Therefore a more detailed evaluation of the process can be performed. Despite the advantages of modeling and simulation, hardly

any studies for the dosator process exist. (Joliffe et al., 1980) investigated the powder retention in the dosator caused by arching. For this purpose, the arching theories for hopper design from (Walker, 1966) and (Walters, 1977) were adapted. High wall friction angles reduce the required compression stress, whilst it increases with higher radius of the dosator nozzle and bulk density. (Khawam and Schultz, 2011) proposed a theoretical model for capsule fill weight predictions. The powder density inside the dosator nozzle is calculated by multiplying the bulk density with precompression and compression factors. However, those factors are not related to any material properties and have to be determined experimentally. Furthermore it is assumed that retention always occurs, since arching behavior is not considered. Also no fill weight variations due to inhomogeneity of the powder bed or improper plug ejection can be predicted.

A simulation of the dosator process was done by (Loidolt et al., 2017). The dosed mass and the pressure inside the dosator during the dipping step were recorded for various CMAs. The results show that the filling of the dosator takes place in three consecutive steps (Fig. 2). In the first step the dosator gets filled linearly, with very little pressure acting on the powder. As soon as the whole dosator chamber has moved into the powder bed, a sharp increase of the pressure is recorded at the start of the second step. In this step the mass remains nearly constant, until the dosator comes close to the bottom (approx. 1 mm). Now the pressure rises again as the powder gets compressed into the dosator nozzle (third step). For highly cohesive powders the boundaries of the steps vanish because additional effects like bridging get more relevant. However, just a qualitative analysis of the process without comparison to experimental data was given. Moreover only the dipping of the dosator into the bed is taken into account, whereas the withdrawal is neglected. Therefore, no considerations about powder retention are possible.

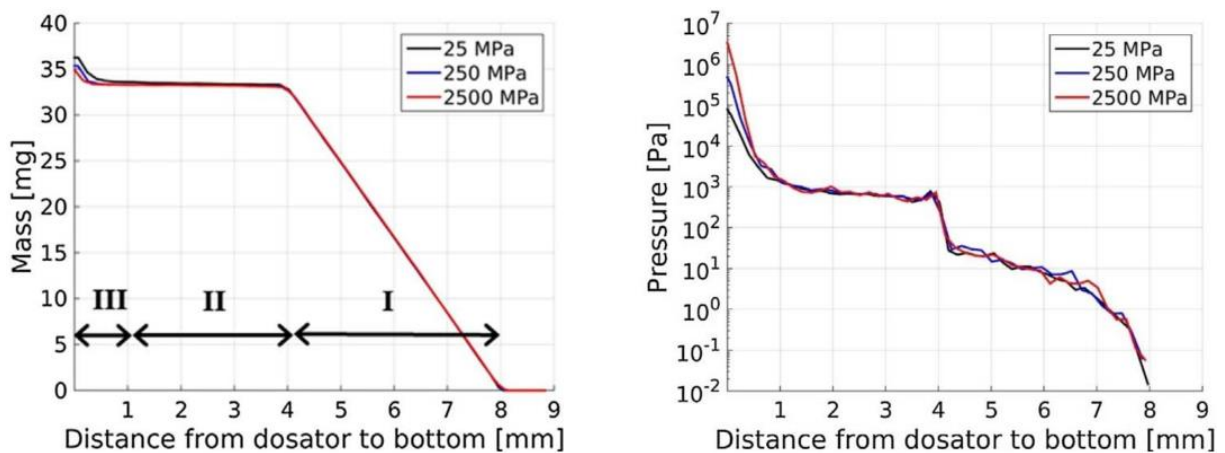


Fig. 2: The three steps of dosator filling: (i) volumetric filling step, (ii) intermediate step and (iii) compression step (Loidolt et al., 2017).

This thesis is intended to be a continuation of the work of (Loidolt et al., 2017), examining parts of the mentioned outlook. First of all the dosator movement is adapted so that the movement out of the bed is considered too. For this purpose the introduction of a velocity profile is necessary for a better replication of reality and to avoid unreasonable high accelerations. Further the suitability of two different contact models for the process is evaluated by comparison of simulation results with experimental data obtained from (Faulhammer et al., 2014a). The influences of machine speed, gap width between dosator nozzle and bottom of the powder bed as well as powder bed height are investigated. Also different dosator geometries were examined. At last the effects of bed inhomogeneity are analyzed by creating powder beds with varying bulk densities.

2 Methods

2.1 DEM

The Discrete Element Method (also Distinct Element Method, DEM) introduced by (Cundall and Strack, 1979) is a numerical simulation method for particle flow. Based on a contact model, the forces acting between touching particles are determined. By solving Newton's second law of motion for every particle, the particle movement is calculated. The open-source software LIGGGHTS® (Kloss et al., 2012) is used for this purpose. It is based on a soft-sphere approach, which assumes spherical particles, and instead of taking particle deformation into account, colliding spheres are allowed to overlap (Fig. 3a). The contact force is calculated with a spring-dashpot model in normal direction and in tangential direction respectively (Fig. 3b). According to (Eq. 1) the normal force F_n consists of an normal overlap δ_n dependent spring force representing the repulsive contact force, a viscous damping force acting in the opposite direction of the relative particle velocity v_n and a constant pull off force F_0 . The normal overlap of the particles equals the sum of the radii minus the distance between the centers of the two spheres (Eq. 2). The tangential force F_t is calculated by a spring force, which models the shear forces, and an additional damping force (Eq. 3). The tangential overlap δ_t takes the tangential displacement of two particles in contact into account. If the Coulomb criterion (Eq. 4) is met, the tangential overlap is updated via Eq. 5 in every time step. Otherwise it is truncated to fulfill the criterion as stated in Eq. 6.

$$F_n = k_n \delta_n - \gamma_n v_n + F_0 \quad 1$$

$$\delta_n = R_1 + R_2 - |\vec{x}_1 - \vec{x}_2| \quad 2$$

$$F_t = -k_t \delta_t - \gamma_t v_t \quad 3$$

$$|k_t \delta_t| \leq \mu F_n \quad 4$$

$$\delta_{t,new} = \delta_{t,old} + v_t \Delta t \quad 5$$

$$\delta_t = \frac{\mu F_n}{k_t} \quad 6$$

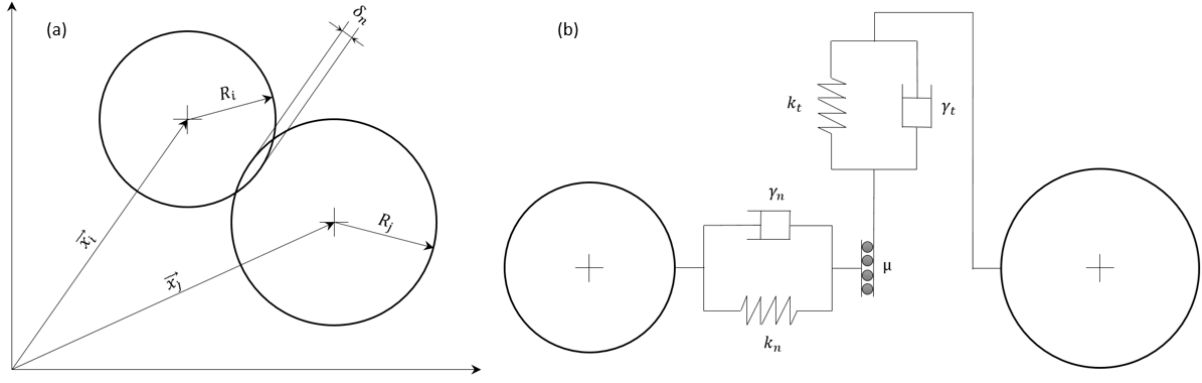


Fig. 3: (a) Collision of two spheres generates an overlap δ_n . (b) Spring-dashpot model in normal and tangential direction, connected via the friction coefficient μ .

2.2 Hertz contact model

The Hertz theory (Hertz, 1881) is a common approach in DEM modeling. The contact force is determined by using effective parameters, which are calculated via the size and material parameters of the respective spheres (Eq. 7 - 10). The stiffnesses k_n and k_t of the springs show a dependency with the normal overlap, leading to non-linear behavior (Eq. 11, 12). The damping coefficients γ_n and γ_t are calculated via (Eq. 13, 14). For more detailed information and further literature see (Kloss, 2016). In addition to the normal force obtained from the Hertz model a cohesion model similar as in (Loidolt et al., 2017) was used. A constant attractive force F_0 is added based on the granular Bond number Bo (Eq. 15). In total, the Hertz model needs seven parameters: particle radius R , density ρ , Young's modulus Y , Poisson ratio ν , coefficient of restitution e , friction coefficient μ and Bond number Bo . A detailed description of how those parameters are determined follows in section 3.2.3.

$$\frac{1}{R_{eff}} = \frac{1}{R_1} + \frac{1}{R_2} \quad 7$$

$$\frac{1}{m_{eff}} = \frac{1}{m_1} + \frac{1}{m_2} \quad 8$$

$$\frac{1}{Y_{eff}} = \frac{1 - \nu_1^2}{Y_1} + \frac{1 - \nu_2^2}{Y_2} \quad 9$$

$$\frac{1}{G_{eff}} = \frac{2(2 - \nu_1)(1 + \nu_1)}{Y_1} + \frac{2(2 - \nu_2)(1 + \nu_2)}{Y_2} \quad 10$$

$$k_n = \frac{4}{3} Y_{eff} \sqrt{R_{eff} \delta_n} \quad 11$$

$$k_t = 8G_{eff}\sqrt{R_{eff}\delta_n} \quad 12$$

$$\gamma_n = -\sqrt{\frac{20}{3}Y_{eff}m_{eff}\sqrt{R_{eff}\delta_n}} \frac{\ln(e)}{\sqrt{\ln^2(e) + \pi^2}} \quad 13$$

$$\gamma_t = -\sqrt{\frac{80}{3}G_{eff}m_{eff}\sqrt{R_{eff}\delta_n}} \frac{\ln(e)}{\sqrt{\ln^2(e) + \pi^2}} \quad 14$$

$$F_0 = -BoF_g \quad 15$$

2.3 Luding contact model

The Luding model (Luding, 2008) makes use of a loading/unloading hysteresis with three different stiffnesses (Fig. 4). The total normal force results as sum of the hysteresis force F_{hys} , a constant attractive force F_0 (pull off force) and a viscous damping force. For the loading case (particles moving towards each other) the hysteresis force increases linear with the overlap (stiffness k_1). In the case of unloading (particles moving away from each other), the hysteresis force decreases with a higher stiffness k_2 . The value of k_2 is calculated via linear interpolation between k_1 and the maximum stiffness \hat{k}_2 , if the overlap is smaller than the plastic flow limit overlap δ_{max}^* (Eq. 16 - 18). For overlaps larger than δ_{max}^* , the stiffness is limited to \hat{k}_2 for both loading and unloading. This accounts for an adaption of the plastic deformation dependent on the contact force and is an approximation to a more realistic non-linear behavior of particle contacts. When the overlap reaches a certain value δ_0 , the hysteresis force turns from repulsive to attractive. The hysteresis force decreases further (increase of attraction) until the intersection of the two unloading curves is reached. After that, the force follows the second unloading curve and the hysteresis force rises with the third stiffness k_c . If the contact doesn't break, but the overlap increases again, the hysteresis force rises with the respective interpolated k_2 value (Eq. 19). The viscous damping force is calculated as damping coefficient γ_n times the negative value of the relative velocity $-v_n$ (cf. Eq. 1). With a constant pull off force, which is added to the normal force, long distance interactions like Van der Waals forces can be taken into account. The damping coefficient is determined via (Eq. 20).

The calculation of the tangential force distinguishes between static friction (Coulomb criterion is met) and dynamic friction. Due to the fact that repulsive as well as attractive

normal forces can occur, the normal force of Coulombs law is modified in such a way that the cohesion forces are subtracted from the actual normal force (Eq. 21). The tangential stiffness and the tangential damping coefficient are determined via the friction stiffness and friction viscosity parameters respectively, which are defined as the fraction of the normal and the tangential values (Eq. 22-23). Altogether, the Luding model uses ten parameters additional to radius and density: loading, unloading and cohesive stiffness, plasticity depth, pull off force, coefficient of restitution, static and dynamic friction coefficients, tangential stiffness and tangential viscosity.

$$\phi_f = \frac{\delta_0}{2R_{eff}} \quad 16$$

$$\delta_{max}^* = 2R_{eff}\phi_f \frac{\hat{k}_2}{\hat{k}_2 - k_1} \quad 17$$

$$k_2 = \begin{cases} \hat{k}_2 & \text{if } \delta_{max} \geq \delta_{max}^* \\ k_1 + (\hat{k}_2 - k_1) \frac{\delta_{max}}{\delta_{max}^*} & \text{if } \delta_{max} < \delta_{max}^* \end{cases} \quad 18$$

$$F_{hys} = \begin{cases} k_1\delta_n & \text{if } k_2(\delta_n - \delta_0) \geq k_1\delta_n \\ k_2(\delta_n - \delta_0) & \text{if } k_1\delta_n > k_2(\delta_n - \delta_0) > -k_c\delta_n \\ -k_c\delta_n & \text{if } -k_c\delta_n \geq k_2(\delta_n - \delta_0) \end{cases} \quad 19$$

$$\gamma_n = \sqrt{\frac{4m_{eff}k_n}{1 + \left(\frac{\pi}{\ln(e)}\right)^2}} \quad 20$$

$$F_{n,Coulomb} = F_n - (-k_c\delta_n + F_0) \quad 21$$

$$f_k = \frac{k_t}{k_n} \quad 22$$

$$f_\gamma = \frac{\gamma_t}{\gamma_n} \quad 23$$

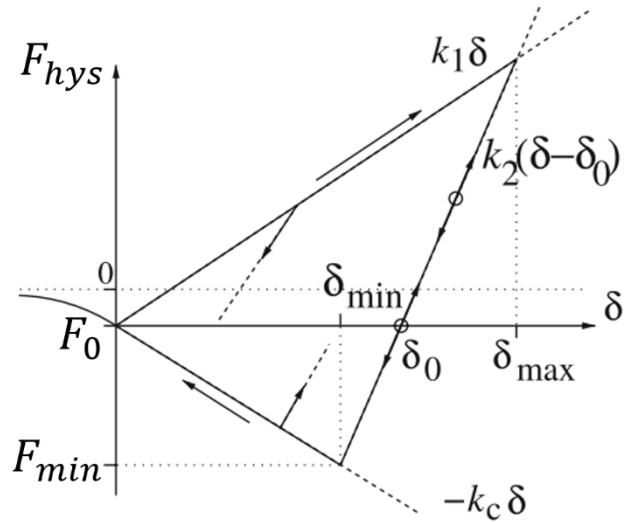


Fig. 4: Normal force hysteresis of the Luding contact model (modified from Luding, 2008).

2.4 Simulation setup

2.4.1 Geometric setup

The simulation of the dosator process is divided into two steps, namely the creation of the powder bed and the actual dosing. During powder bed creation particles are randomly placed in a simulation box with periodic boundary conditions in x- and y-direction. The particles settle at a static wall at the bottom of the box due to the influence of gravity. An initial velocity in z-direction is assigned to every single particle. They are also exposed to a drag force, which limits the settling velocity to the value of the initial velocity. This settings ensure a homogeneous bed with a certain bulk density. The powder bed can be used as a starting point of subsequent dosing simulations with different process parameters. A certain powder bed height can simply be set by deleting all particles which are above the desired powder bed height. The multiple usage of the initial powder bed causes an enormous reduction of the computational effort.

During dosing simulation the dosator is loaded into the simulation box and moves into the powder bed, until a predefined clearance to the bottom is reached (herein after also referred to as gap width). After that the dosator moves out of the powder bed until it reaches the starting position. No additional compression with the piston inside the dosator is used, since it was also omitted in the experiments of (Faulhammer et al., 2014a), which were used for validation. During the dosing, the height of the lower edge of the dosator above the bottom wall (dosator position), as well as the mass and the pressure inside the dosator are recorded. Fig. 5 shows a cross section of the dosator and the powder bed. Since different

dosator geometries and powder bed heights are simulated, two dimensionless quantities are introduced, which make the comparison of the results possible. On the one hand the dosator position is normalized with the powder bed height, taking the gap width z_e as reference point (Eq. 24). On the other hand the bulk density inside the dosator is normalized with the particle density (density of the material), yielding a relative density (solid fraction) of the powder inside the dosator chamber. The bulk density is calculated as dosed mass divided by the dosator volume (Eq. 25). For all cases without variation of the powder bed height and gap width, the normalized dosator distance and the absolute position are equivalent measures, since every run has the same starting point and end point. If the dosator geometry remains unchanged, the same accounts for the relative density and the dosed mass.

$$z_{rel} = \frac{z - z_e}{h - z_e} \quad 24$$

$$\rho_{rel} = \frac{\rho_{bulk}}{\rho_{particle}} = \frac{4 * m}{d^2 * \pi * cl * \rho_{particle}} \quad 25$$

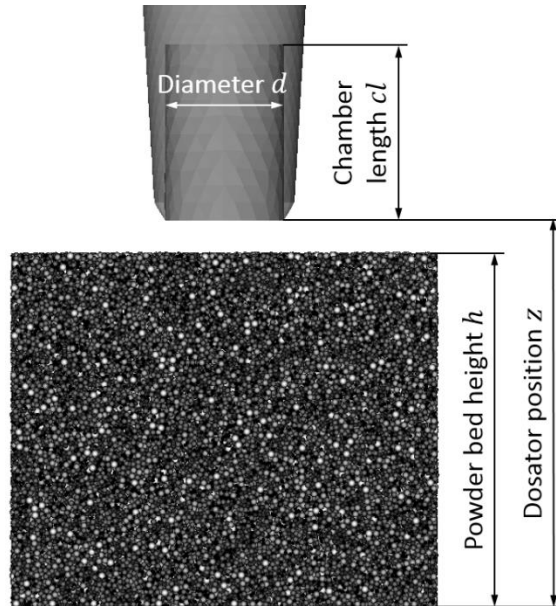


Fig. 5: Cross section of the geometrical setup. Small particles are black, large particles are white.

2.4.2 Dosator movement

Since the exact velocity profile of the real dosator machine is not known, it is assumed to be sinusoidal (Eq. 26). The dosator position z is given by Eq. 27. The amplitude \hat{v} of the velocity v and the angular frequency ω depend on the machine speed n , i.e. the amount of capsules

produced per hour. The chosen amplitude is obtained from measurements of the mean velocity \bar{v} (Eq. 28). During one full rotation (one produced capsule) the dosator has to move up and down twice, once for the dosing and the second time for the capsule filling. Due to a lack of detailed information it is assumed, that both movements take equally long. Therefore the angular frequency can be calculated via Eq. 29. The phase shift θ is determined from the starting position of the dosator z_0 (1 mm above the powder bed with the height h) and the clearance at the bottom z_e (Eq. 30). In Table 1 the parameters for the velocity profile are shown.

$$v(t) = \hat{v} \sin(\omega t + \theta) \quad 26$$

$$z(t) = z_e - \frac{\hat{v}}{\omega} (\cos(\omega t + \theta) - 1) \quad 27$$

$$\hat{v} = \bar{v} \frac{\pi}{2} \quad 28$$

$$\omega = 4\pi n \quad 29$$

$$\theta = \arccos\left(\frac{(z_0 - z_e)\omega}{\hat{v}} - 1\right) + \pi \quad 30$$

Table 1: Parameters of the velocity profile for different machine speeds, powder bed heights and gap widths.

n $\left[\frac{\text{capsules}}{\text{hour}}\right]$	\bar{v} $\left[\frac{\text{mm}}{\text{s}}\right]$	\hat{v} $\left[\frac{\text{mm}}{\text{s}}\right]$	ω $\left[\frac{1}{\text{s}}\right]$
500	71.5	112.31	1.75
1500	214.5	336.94	5.24
2500	357.5	561.56	8.73
h [mm]	z_0 [mm]	z_e [mm]	θ [-]
3.75	4.75	0.6	2.847
5	6	0.2	2.793
5	6	0.4	2.799
5	6	0.6	2.806
5	6	0.8	2.812
5	6	1	2.818
7.5	8.5	0.6	2.734
10	11	0.6	2.673
12.5	13.5	0.6	2.619

3 Verification, calibration and validation

Nowadays many different simulation approaches with different models are used. A model of any real system is always a simplification in some way. It depends on the purpose or the goal of a simulation, which simplifications are acceptable and which not. It has to be ensured, that the results of the simulations are satisfactory. Extensive testing of the used software and the models is therefore necessary. Since it is often impossible or at least costly in terms of time and money to get absolutely valid models, the effort spent for testing is always dependent on the necessary degree of confidence in the model (Sargent, 2007). In general, the testing of simulation software can be divided in two main parts, namely verification and validation. Verification ensures that the implementation of the software and the models is correct (i.e. the code does what it should do). For this purpose simulation results are usually compared to analytical solutions. In a broader sense verification includes testing the source code and the whole software to eliminate implementation errors. A third party software is used in this work, and therefore only verification of the used contact models is done. In the validation step, the models are tested for the ability to represent the real system. Usually validation includes the replication of experiments and comparison of the results. In general, the correctness of the model can only be ensured within the validated range of parameters, i.e. no extrapolation is possible. In order to make a successful validation possible, the parameters of the contact model usually have to be determined in a calibration procedure. Detailed information on verification and validation of simulation models can be found in (Kleijnen, 1995; Sargent, 2007).

3.1 Verification

The simulation results were compared to analytical solutions during verification of the Hertz model and the Luding model. The normal models were evaluated for a single particle-particle contact and a particle-wall contact. One particle with a predefined initial velocity was placed above a spatially fixed particle or a fixed wall respectively (Fig. 6a). Every model was evaluated for three different cases. In case one and two the damping force was turned off but in case three damping was used. In the first case the initial velocity was chosen high enough that the particle bounced off after contact. In contrast to that a lower initial velocity is used in the second case and thus the particle stays in contact. The third case shows the contact force including a damping force according to Eq. 1. Only the first case was reproduced analytically, but a qualitative analysis shows the plausibility of the results for the other two cases.

For the verification of the tangential models, a particle was allowed to settle on a wall until the particle-wall contact is in equilibrium, i.e. the contact force equals zero and the normal overlap remains constant (Fig. 6b). Now the particle is charged with an initial velocity in tangential direction (parallel to the wall). The recorded results for the normal model simulation are the normal contact force and the overlap, whereas for the tangential model the tangential force and the particle velocity were observed.

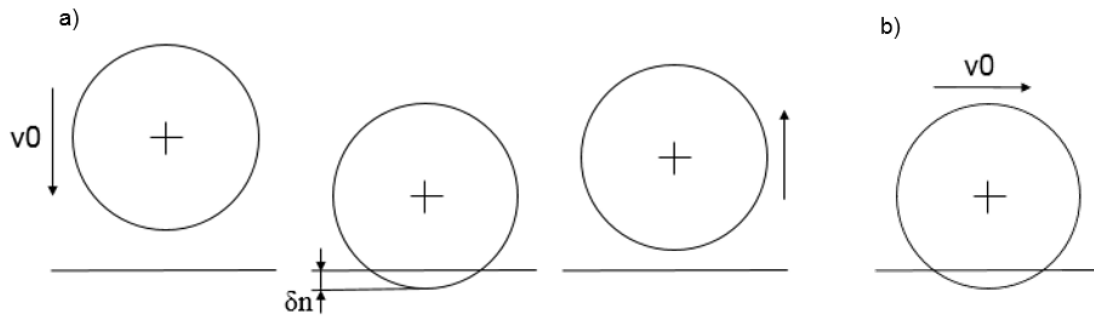


Fig. 6: Verification setup for the (a) normal model and (b) tangential model.

3.1.1 Hertz normal model

In Fig. 7a the results of the verification of the Hertz normal model for particle-particle contact are shown. Evidently the simulation results of the first case agree with the analytical solution. The second case is not shown in this figure for the sake of clarity. However, the contact force oscillates along the force function, until the equilibrium state is reached, in which the force equals zero. In the third case, when the viscous damping force is active, the contact force is increased for the loading part, otherwise it is decreased. Thus the damping force always acts as expected against the direction of the particle velocity. Fig. 7b shows the same results for a particle-wall contact. Noticeable are the differences of the contact force and overlap compared to the particle-particle contact. This behavior can be attributed to Eq. 7, where the radius of the wall is set to infinity. Therefore the effective particle radius is twice as large as it would be for equal sized particles. The same effect is responsible for the higher cohesion force, which is calculated via the volume of the reduced sphere, leading to an eight times larger force. This behavior can easily be avoided by adjusting the material properties of the wall.

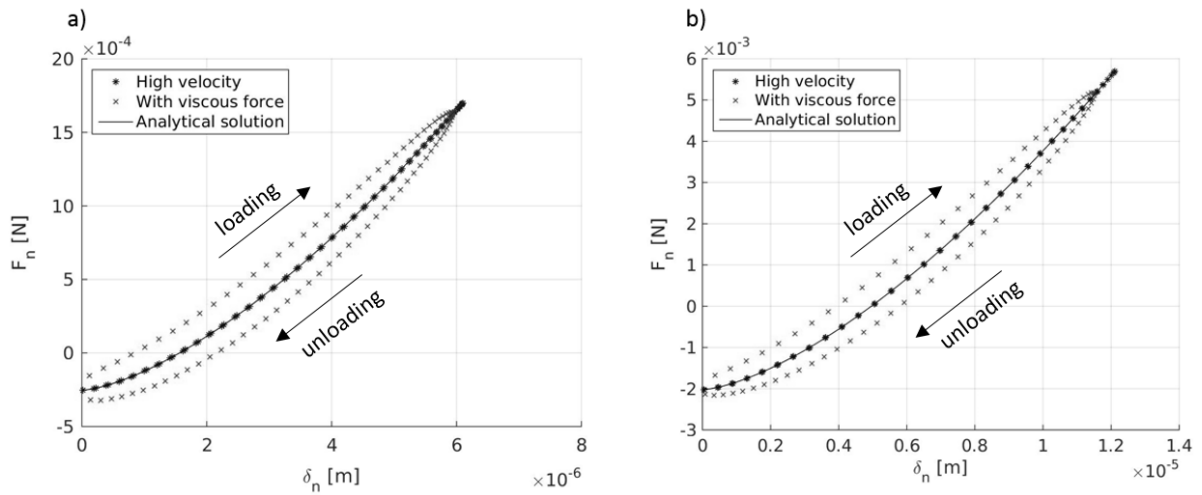


Fig. 7: Contact force of (a) a single particle-particle contact and (b) a particle-wall contact with and without damping force for the Hertz normal model.

3.1.2 Hertz tangential model

The results of the verification case for the Hertz tangential model coincide with the analytical solution (Fig. 8). At the first step the tangential overlap equals zero, therefore the initial tangential force is determined by the damping part of Eq. 3. With increasing tangential overlap the force magnitude increases, resulting in a sharp decrease of the velocity. When the shear force exceeds the Coulomb criterion, the tangential overlap is adjusted in a way to keep the tangential force constant. As soon as the particle velocity changes its sign, the tangential overlap is updated by integration over time again. In reality the particle velocity would decrease gradually until the particle doesn't move anymore. Due to the nature of the spring-dashpot model the particle velocity can oscillate in the simulation before the velocity converges to zero.

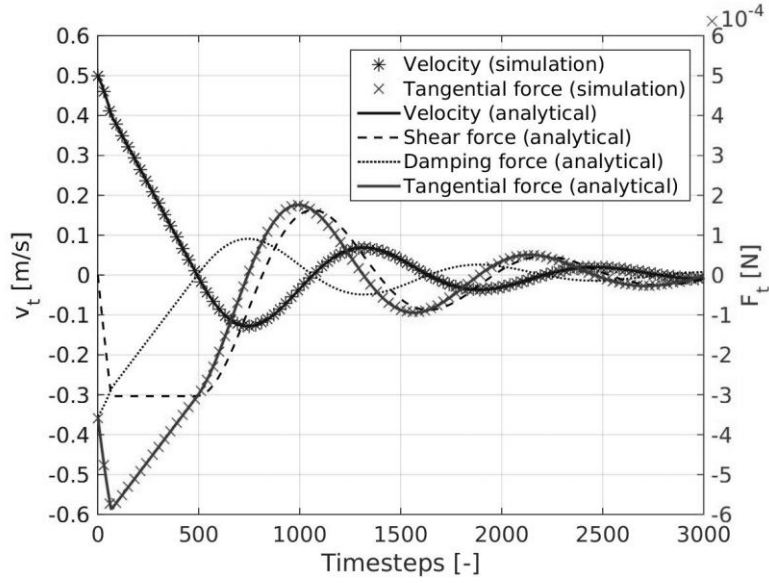


Fig. 8: Tangential force and particle velocity for the Hertz tangential model.

3.1.3 Luding normal model

The verification cases of the Luding normal model for particle-particle contact (Fig. 9a) and particle-wall contact (Fig. 9b) confirm the proper functionality. For a high initial velocity, the contact force increases linear with the loading stiffness k_1 until the plastic flow limit δ_{max}^* is reached. Beyond that the maximum stiffness \hat{k}_2 is used, which furthermore determines the contact force in the unloading case towards the intersection point with the cohesion force. The second case with a lower initial velocity shows the interpolation of the unloading stiffness, which is calculated with the current overlap. The densification of data points indicates a low particle velocity as well as an oscillation until the equilibrium state at zero force is reached. In the third case the viscous damping force is active, which leads to an additional force opposed to the direction of the particle movement. Similar to the Hertz model the effective radius of the contact is doubled for a particle-wall contact, but in this model the pull off force is not size dependent.

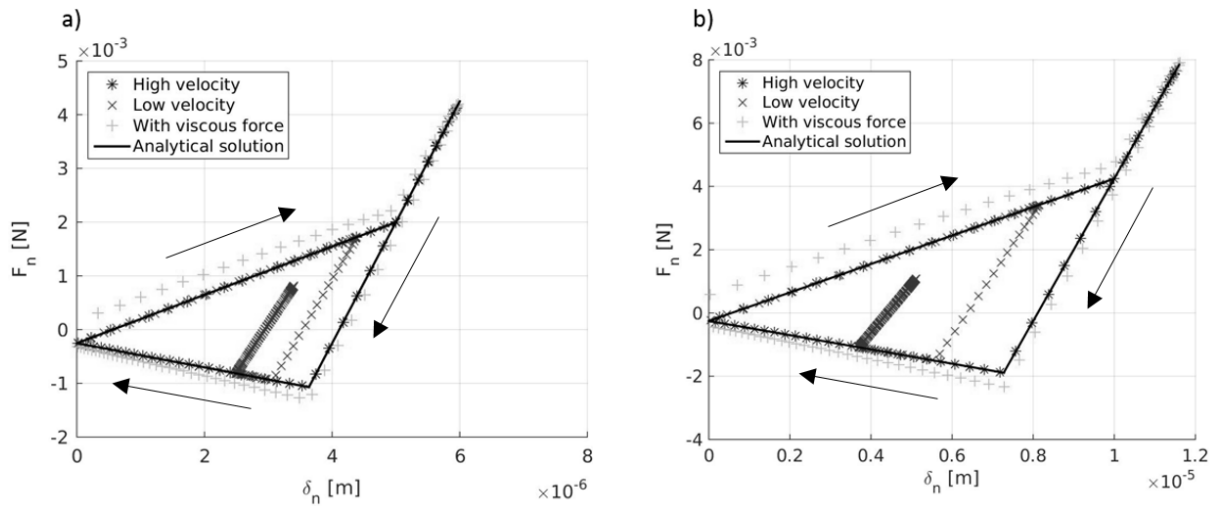


Fig. 9: Contact force of a single particle-particle contact (a) and a particle-wall contact (b) with and without damping force for the Hertz normal model.

3.1.4 Luding tangential model

The Luding tangential model is based on the same principles as the Hertz model, but there are differences regarding the determination of the model parameters. An extension is the implementation of dynamic friction. When the Coulomb criterion is met, the tangential overlap is truncated with respect to the dynamic friction coefficient instead of the static one. Therefore the shear force jumps to a lower level. Now the Coulomb criterion is fulfilled again and so the tangential force is calculated in the usual manner (Fig. 10). Regarding this behavior an adaption of the model is proposed for the future: In the current implementation the tangential overlap is integrated over time as soon as the shear force is reduced in case the dynamic friction becomes active. From mechanical point of view it would make more sense to hold the overlap constant until the spring force is lower than the dynamic friction force.

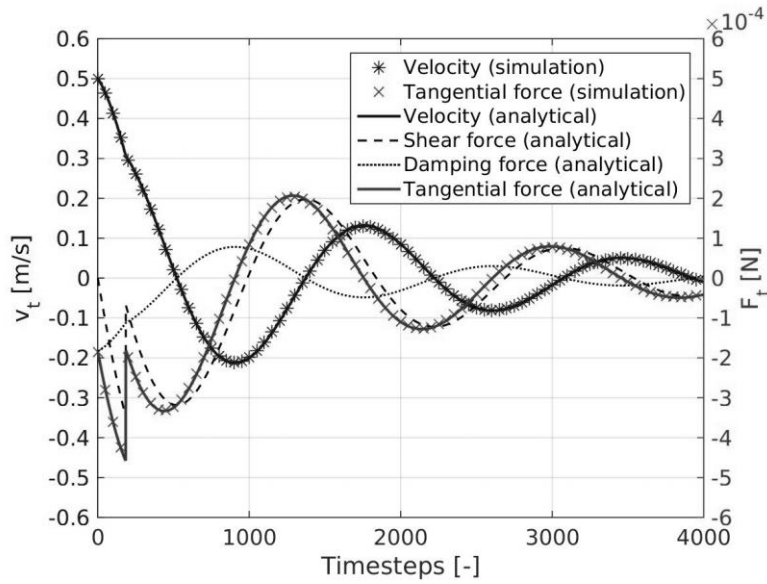


Fig. 10: Verification of the Luding tangential model.

3.2 Calibration of model parameters

3.2.1 Fundamentals of model calibration

According to (Marigo and Stitt, 2015), the applicability of DEM for industrial use is mainly dependent on the calibration of the model parameters. In general, two ways are possible for the calibration of the contact model. On the micro scale the Direct Measuring Approach exists. The physical properties of the material like Young's modulus, Poisson ratio, coefficient of restitution or friction coefficient are directly obtained from measurements. Although this seems to be a somehow straightforward procedure, it comes along with some restrictions. First of all the used contact model has to be based on these physical quantities. This is the case for the Hertz model, but not for the Luding model. Furthermore it is not always possible to measure those properties, especially for small and irregular particles. And even though the Hertz model is principally based on physical quantities, not every parameter is necessarily linked to a real quantity, especially when rolling friction or cohesion models are used.

On the other hand the Bulk Calibration Approach is used for macro scale calibration. The goal is to choose the model parameters in a way that the bulk behavior is the same as the one of the real powder. For this purpose different tests with measurable quantities, for example hopper discharge, angle of repose or rheometer experiments are defined. Those experiments are replicated in the simulation by changing the model parameters iteratively until a sufficient result is obtained. No correlation between model parameters and physical

quantities exists in this case. Due to the macroscopic approach, different sets of parameters can be able to reproduce the bulk response. This parameter space decreases with a higher number of experiments (Coetzee, 2017).

Although the Bulk Calibration Approach is widely used in industry, no standard procedure for the determination of the contact model parameters exists, but calibration of the model is necessary to obtain reasonable results (Asaf et al., 2007). Trial and error is still the most common approach despite many disadvantages. Since it lacks a structured strategy many runs may be necessary until sufficient accuracy is obtained. The success is often dependent on the experience of the user and for a higher number of contact parameters this method gets quite unpractical. Furthermore there is no guarantee that the chosen parameters lead to the best achievable result and it is hardly possible to increase process understanding (Rackl and Hanley, 2017). A more systematic approach is the so-called one factor at a time method (OFAT), in which one factor is varied in every run. This method allows the determination of the influence of every respective parameter on the output (also referred to as main effects). However, no interaction effects can be taken into account, as for example the loading and unloading stiffness of the Luding model may interact with each other. Therefore a more sophisticated approach would be helpful, which is provided by the Design of Experiments (DoE) method.

3.2.2 Design of Experiments

DoE, introduced by (Fisher, 1936), was originally developed for process optimization, but the principles can also be applied to the calibration procedure for DEM simulations, as done by (Johnstone, 2010; Pantaleev et al., 2017; Wilkinson et al., 2017). It allows not only to determine the influence of the main effects, but to resolve interactions between model parameters in a reasonable number of runs. There are three aspects taken into account in the process: factors, levels and the response. Factors are the variable inputs which influence the experiment. In DEM the contact model parameters are factors. Levels are the respective values of each factor and the response is the output of the experiment (or simulation). For a low number of factors and levels a full factorial design can be used, meaning that every possible combination of values is tested. The number of runs necessary for a full factorial design is equal to l^f , where l is the number of levels, and f is the number of factors. Due to the exponential relationship, the number of levels is usually low, in most cases only two levels are chosen. With this restriction a linear impact of the factors on the response is assumed, whereas a parabolic effect could be described in case of three levels. In the following context only two level designs are considered.

For a high number of factors (five or more) usually a fractional factorial design is applied to avoid too many runs. In contrast to the full factorial design, which is able to resolve every single interaction independently, the reduction of runs comes along with confounded interactions. However, usually the main effects and second order interactions (interactions of two factors) are most relevant for the response, while higher order interactions are playing a minor role. The resolution of a design gives information about how main effects are confounded with higher order interactions. It is calculated by adding one to the smallest order any main effect is confounded with (denoted by Roman numerals). If the main effects are confounded with fourth order and higher interactions, the resolution is V. With a resolution of V or higher, it is also ensured, that second order interactions are not confounded with each other. In case of a resolution IV second order interactions can be confounded. Therefore designs with a resolution of V should lead to excellent results, but a resolution of IV may also be adequate for many cases. A resolution of III should be avoided since the main effects are confounded with second order interactions. They are only applicable for screening designs with a high number of factors to determine which ones have significant impact on the response.

Based on the results of the particular runs an equation for the response can be derived by linearization between the levels of each factor (Eq. 31). The average is the arithmetic mean of all results. The effect of a factor can be calculated as the difference of the arithmetic means of all runs with high level of the factor and the ones with low level. For interactions the high level can be determined by multiplying the high levels of all interacting factors, the same accounts for the low levels. For example, the interaction between the factors A and B has the high level $AB_{high} = A_{high} * B_{high}$. With Eq. 31 it is possible to predict the response depending on the factors, which can be used for calibration. The factors are restricted to the range between the low and high level. If different experiments are carried out for calibration, a simulation design matrix based on DoE principles can be generated and the response equation can be derived for every experiment. Then an optimization procedure can be used to find the best fitting model parameters.

$$Response = average + \sum \frac{effect}{high\ level - low\ level} * value \quad 31$$

3.2.3 Applied calibration procedure

A combination of the Direct Measuring Approach and the Bulk Calibration Approach is used in this study. As suggested by (Coetzee, 2017), at first the particle size and shape were

defined. These two parameters affect all the other ones, and a change would imply that the calibration procedure has to be restarted. The particle size distribution is roughly based on the size parameters of the powder Lactohale 100 stated in (Stranzinger et al., 2017), though a symmetric distribution with five classes between 100 μm and 220 μm was chosen (Fig. 11). The mean diameter is 160 μm . Spherical particles are assumed for all simulations. With this setup up to 700.000 particles were simulated. The solid density of Lactohale 100 is given with 1539 kg/m^3 . Those parameters were defined independently of the contact model by using the Direct Measuring Approach. All other parameters were obtained by making use of the Bulk Calibration Approach for each model.

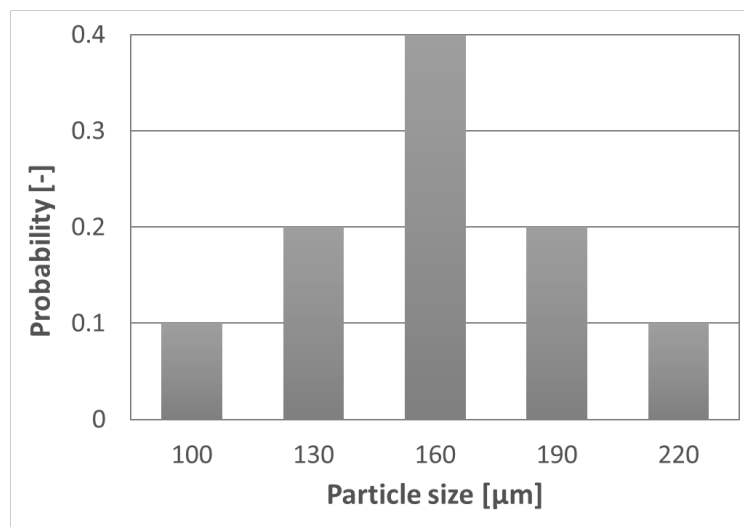


Fig. 11: Particle size distribution

As described above, the inserted particles are given an initial settling velocity. Its value has substantial impact on the bulk density of the particle bed, which is comparable to different heights of drop as investigated by (Macrae and Gray, 1961). Therefore the settling velocity is considered to be a significant factor in addition to the model parameters. Since the powder in the real dosator is exposed to machine vibrations, it can be assumed that the density of the bed is somewhere in the range of the tapped density, which is approximately 820 kg/m^3 according to (Faulhammer et al., 2014a).

For the calibration of the Hertz model the parameters of (Loidolt et al., 2017) were used as start value. The value for Young's modulus wasn't changed, since a higher stiffness would require a smaller timestep and therefore more computational effort. On the other hand no further reduction was possible due to a restriction of the used software. Reducing particle stiffness is a common approach to increase the size of the timestep (Lommen et al., 2014;

Malone and Xu, 2008). A DoE study of the simulation bulk density including the remaining model parameters and the initial settling velocity was performed. It showed that the settling velocity and the Bond number are the main factors for the bulk density. For this study a smaller simulation domain was used in order to reduce the amount of particles. Ten different Bond/velocity pairs were tested and three of them delivered sufficient bulk densities. With each pair three simulations with different dosator geometries were run and compared to the experiments of (Faulhammer et al., 2014a). The best agreement was observed for an initial settling velocity of 0.6 m/s and a Bond number of 400. Then the other parameters were optimized via DoE to find the best parameter set. The resulting bulk density was 807.6 kg/m³. The iterative procedure with small geometric setups for the determination of the bulk density based on DoE allowed a rather fast determination of the contact parameters with a reasonable amount of runs. The calibration with three dosator geometries was necessary to find one unique parameter set with general validity which applies for all three cases. The obtained values for the parameters are stated in Table 2.

Table 2: Model parameters for the Hertz model determined with the Bulk Calibration Approach

Y [MPa]	ν [-]	e [-]	μ [-]	Bo [-]	v_{set} $\left[\frac{m}{s}\right]$
25	0.3	0.45	0.5	400	0.6

In contrast to the Hertz model the calibration of the Luding model was way more challenging. No initial values were known and a DoE with eleven factors and a resolution of IV for three different dosator geometries would require a total of 96 simulations. For those simulations a high and low level value has to be guessed first, possibly leading to completely wrong starting values. With that in mind only the five parameters which are necessary for the calculation of the normal spring force and the settling velocity were considered in the first step. The other five parameters were set to 0.5. Then the effects of the factors on the bulk density were determined. Based on those results the values of the pull off force, plasticity depth and settling velocity were fixed. Then a full factorial DoE was executed with the three stiffness parameters for each of the three dosator geometries. After the best fitting values were found, a simple OFAT approach was used to optimize the parameters for damping and tangential forces. With a settling velocity of 0.8 m/s a bulk density of 819.1 kg/m³ was obtained. Table 3 shows the parameters for the Luding contact model.

Table 3: Model parameters for the Luding model determined with the Bulk Calibration Approach

$k_1 \left[\frac{N}{m} \right]$	$k_2 \left[\frac{N}{m} \right]$	$k_c \left[\frac{N}{m} \right]$	$\phi_f [-]$	$F_0 [N]$	$e [-]$	$\mu_s [-]$	$\mu_d [-]$	$f_k [-]$	$f_\gamma [-]$	$v_{set} \left[\frac{m}{s} \right]$
100	800	33	0.05	-10^{-5}	0.8	0.8	0.3	0.8	0.2	0.8

(Coetzee, 2017) recommends to use different experiments for contact model calibration than the one which is investigated, if the goal of the simulation is to support process development and design. Since the objective of this work is the improvement of process understanding and nothing else than parameter sensitivity studies are executed, the same experiment can be used. However, the calibration of the powder with standardized experiments, for example rheometer tests, is part of future work.

3.3 Validation

For the validation of the contact models experimental results of (Faulhammer et al., 2014a) for Lactohale 100 were used. In total twelve different simulations were run for each model, using the same process parameters as in the experiments: The machine speed is varied between 500 and 2500 capsules per hour, the dosator diameter from 1.9 mm to 3.4 mm, the dosator chamber length is between 2.5 mm and 5 mm and the powder bed height ranges from 5 mm to 12.5 mm. Table 4 shows the different settings and the results both of the experiments and the simulations, as well as the relative deviations.

Table 4: Results of the validation runs for both contact models. The Luding contact model shows better agreement with the experimental data obtained from (Faulhammer et al., 2014a).

Run	Setting				Experiment			Hertz model		Luding model	
	n	d	cl	h	m	m	Deviation	m	Deviation		
[-]	[cph]	[mm]	[mm]	[mm]	[mg]	[mg]	[%]	[mg]	[%]		
1	2500	1.9	2.5	5	6.0	5.5	-7.99	5.7	-5.03		
2	500	1.9	2.5	5	5.7	5.6	-2.01	5.6	-1.32		
3	2500	1.9	2.5	12.5	6.3	5.6	-11.31	5.8	-7.40		
4	2500	1.9	5	10	10.4	10.1	-2.93	10.6	1.97		
5	500	1.9	5	12.5	10.6	8.9	-16.39	10.5	-1.07		
6	1500	2.8	3.75	10	19.0	19.3	1.70	19.5	2.83		
7	500	3.4	2.5	5	19.8	19.1	-3.56	19.4	-2.05		
8	2500	3.4	2.5	5	19.9	19.1	-4.07	19.6	-1.70		
9	2500	3.4	2.5	12.5	21.3	19.2	-9.77	20.0	-6.28		
10	500	3.4	2.5	12.5	20.9	19.1	-8.56	19.9	-4.94		
11	500	3.4	5	10	35.6	38.4	7.92	39.0	9.49		
12	2500	3.4	5	12.5	37.3	38.5	3.24	39.4	5.61		

The simulation with the Hertz model partially shows large errors with a maximal deviation of more than 16 %. Especially for the largest powder bed height of 12.5 mm extensive deviations occur, with exception of the last run. Furthermore it can't be assumed that the results are representative for small dosator diameters as can be seen for the first three runs with the same dosator geometry. The simulation run 2 shows a higher mass than run 1 and the same mass as run 3, which is not in agreement with the experimental results. The same applies for runs 4 and 5. Therefore the Hertz model is not suitable to reproduce the dosator process. An improved cohesion model combined with more extensive model calibration could possibly lead to better validity.

For the Luding contact model all deviations between simulations and experiments are below 10 %. The average difference is 4.1 % compared to 6.6 % for the Hertz model. It is conspicuous that all deviations for a chamber length of 2.5 mm are negative, whilst they are positive for 5 mm chamber length except for run 5. The reason for this effect could be that the wall friction or wall cohesion parameters are set too low. Since already ten model parameters had to be determined, no differentiation between material properties of the powder and the wall has been considered. Regarding the qualitative representation of the process, the simulation results with the Luding model generally are in accordance with the experimental data. Only the mass of run 5 is lower than the one of run 4, which is not conform to the experiments. Since the machine speed and the powder bed height are different in those runs, it could be possible that the interaction of those parameters is not sufficiently represented in the simulations. However, the discrepancy is very small, as are the relative deviations of both runs. All in all the Luding model is valid for a qualitative simulation of the dosator process for low cohesive powders. As stated in (Loidolt et al., 2017; Stranzinger et al., 2017), dosing of strong cohesive powders can lead to different behavior. Therefore further calibration and validation would be necessary, if such powders should be investigated.

With both contact models two issues occurred. When the dosator moves into the powder bed, the powder is compressed into the chamber. When the nozzle comes close to the container bottom the particles can't escape, resulting in a fairly high overlap. Therefore, high contact forces occur, which lead to an expansion of the powder when the dosator moves out of the bed. Not all particles, which were trapped during the dipping step necessarily stay in the dosator. The reason for this behavior lies in the modeling approach which omits particle deformation or breakage and the high overlaps always lead to high repulsive forces. This effect is more apparent for the Hertz model, while the hysteresis in the Luding model overcomes this problem to a certain extent, if beneficial values for the plasticity depth and the unloading stiffness are chosen. The second issue, pictured in Fig. 12, is that the powder

plug extends the dosator chamber due to cohesive bonds. If the powder plug would be ejected into the capsule body, the dosed mass would be too high. According to (Faulhammer et al., 2014a) this also happens in experiments, where a nozzle cleaning unit can be used to remove adhering powder. In the simulations only the particles with its center point inside the dosator nozzle contribute to the mass. Although both effects have an impact on the capsule fill weight, they are neglected, because sufficient results were obtained.

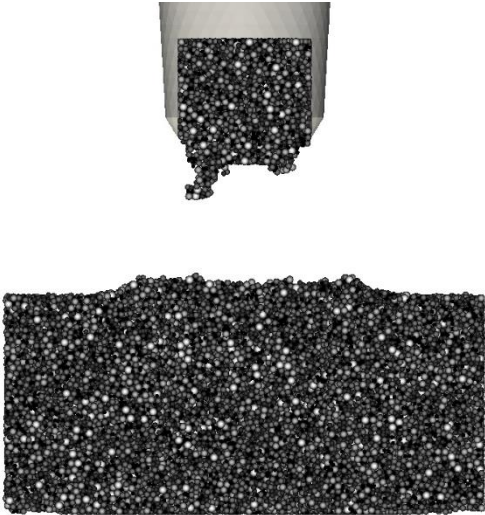


Fig. 12: Powder plug inside the dosator after the dipping step.

4 Results

For the variations of CPPs presented in this section, validation run 8 of the Luding model was chosen as reference case, since it agrees well with experimental data. The runs 2 and 5 show even better agreement, but the high machine speed and low powder bed height of run 8 lead to less computational effort. All parameters which are not explicitly stated are equivalent to the ones in the validation run 8. DoE was not used for the investigation of the process parameters despite the advantages previously mentioned due to the following considerations:

- The focus of this work is the determination of the impact of CPPs on the process, i.e. the main effects, but interactions are of minor interest. DoE is especially advisable for process optimization, as it was done during calibration of the contact model parameters. To get an overview of the process, using OFAT is fine.
- In section 4.4, the dosator geometry is varied in different ways. If this investigations would be based on DoE, the respective factors would not be mutually independent (no orthogonal simulation matrix) and therefore a separated determination of the effects is not possible.
- For the number of factors, only a fractional factorial design with two levels would provide a reasonable amount of simulations due to the exponential scaling of DoE runs. With the OFAT method it is possible to test every factor with several different values, the computational effort still remains feasible.

4.1 Machine speed

In Fig. 13 the evolution of the relative density and the pressure inside the dosator for three different machine speeds (500, 1500 and 2500 capsules per hour) are pictured. One might expect that higher accelerations could affect powder retention, or higher machine speed could reduce bridging effects due to higher shear forces. Actually, the machine speed does not seem to have a significant impact on the dosed mass, which is in accordance with the results obtained by (Faulhammer et al., 2014a). For microcrystalline cellulose, (Llusa et al., 2013) recorded the effect of capsule fill speed on machine vibrations. With increasing speed the powder bed is densified due to the vibrations, leading to higher fill weights. There was no possibility to consider machine vibrations in the current study. Regarding the filling behavior, the three stages of dosator filling proposed by (Loidolt et al., 2017) occur, even though a different contact model is used. The first stage is volumetric filling, in the intermediate second stage the mass remains nearly constant and in the third stage the

powder is compressed. The sharp increase in pressure between the first and second stage is depicted too.

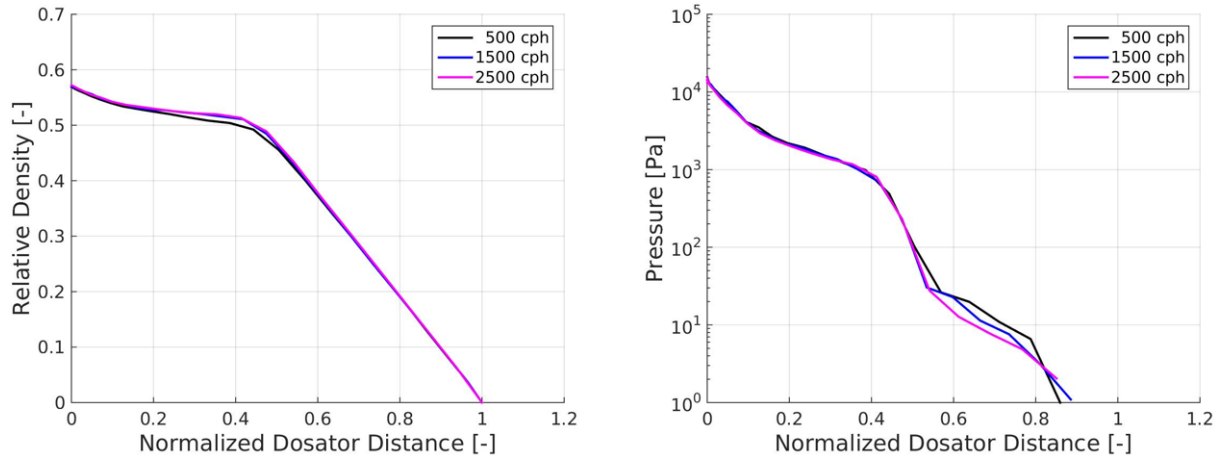


Fig. 13: Relative density and pressure inside the dosator for different machine speeds.

4.2 Powder bed height

Obviously the variation of the powder bed height modifies the precompression ratio (ratio of powder bed height to chamber length), since the chamber length is kept constant. The height is varied between 3.75 and 12.5 mm, leading to precompression ratios between 1.5 and 5. The results show an increase of dosed powder with higher powder beds. In Fig. 14 the density and pressure are pictured both with normalized and absolute dosator position. The top right diagram shows that the filling stages are essentially the same for every case. For high powder beds, the first stage is comparable short compared to second stage. For the smallest bed with 3.75 mm the second stage is nonexistent, the compression starts immediately after filling or maybe even a little bit earlier. Since the mass does not remain absolutely constant in the second stage, but slightly increases, a longer intermediate stage is one reason why the dosed mass increases with powder bed height, albeit it plays a minor role. Interestingly there is a point in the normalized diagram, where all cases coincide. The dotted line between the two diagrams shows that this point is approximately at the start of the third stage. Evidently the compression stage starts earlier for higher powder beds, and therefore the powder in the dosator is more densified. This effect can also be observed in the pressure diagrams.

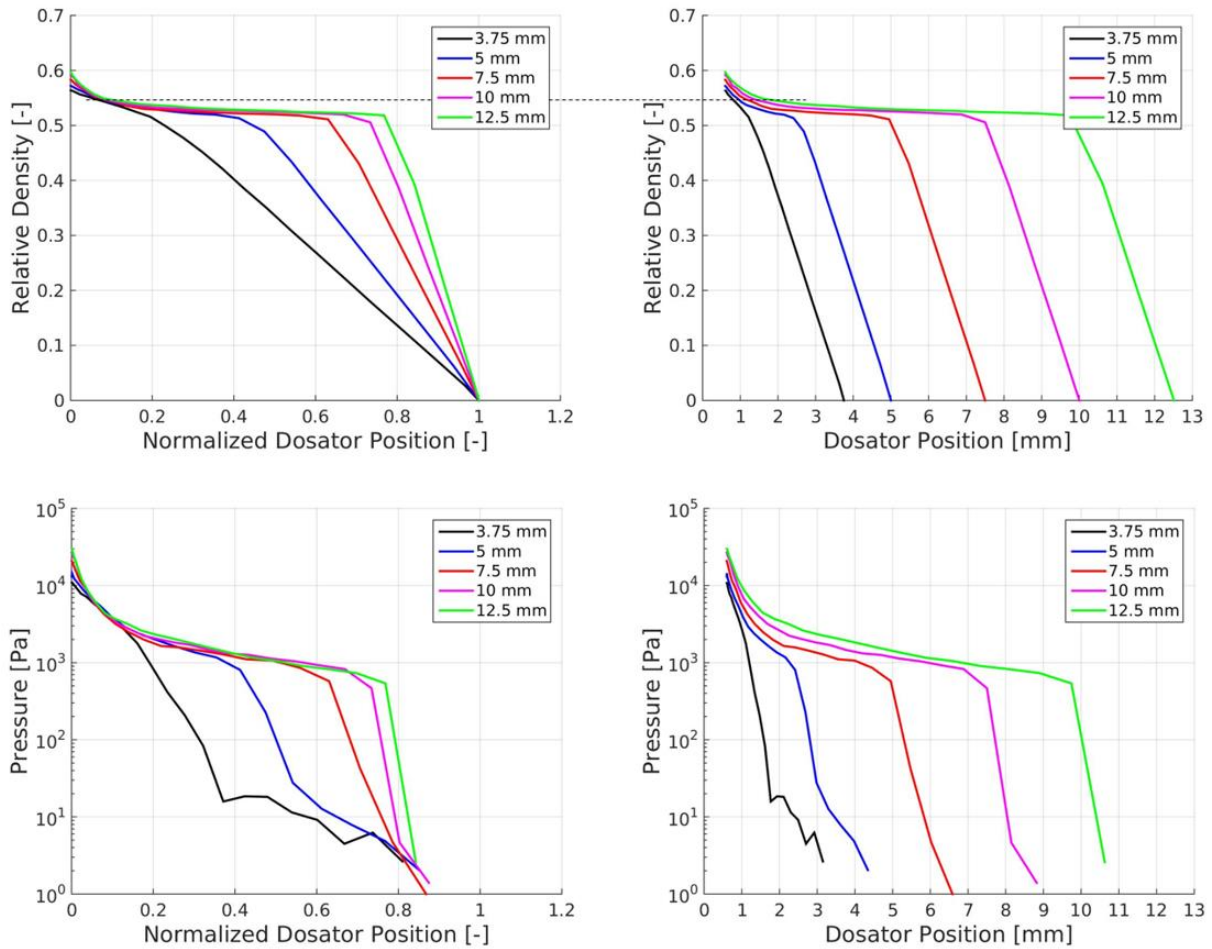


Fig. 14: Relative density for different powder bed heights over the normalized dosator position (top left) and the absolute position (top right), as well as the pressure inside the dosator over the normalized dosator position (bottom left) and the absolute position (bottom right).

4.3 Gap width

Fig. 15 pictures the results of the simulations with a different gap width (0.2 to 1 mm). As expected there is no difference regarding the filling behavior, but the runs with greater gap width simply stop earlier and therefore the mass decreases. For better visibility the end points of the respective runs are marked with an 'x' in the diagrams. Remarkable is that the pressure of the lowest gap width is more than an order of magnitude larger than the one of the highest value. A further increase of the gap width would come along with lower pressure in the dosator. If the critical compression stress is met, powder retention is no longer possible, as described by (Tan and Newton, 1990a). On the other hand with a rather small gap width a highly compressed plug is created. Those plugs can lead to a blockage of the dosator piston when it is tried to eject them into the capsule (Faulhammer et al., 2014a).

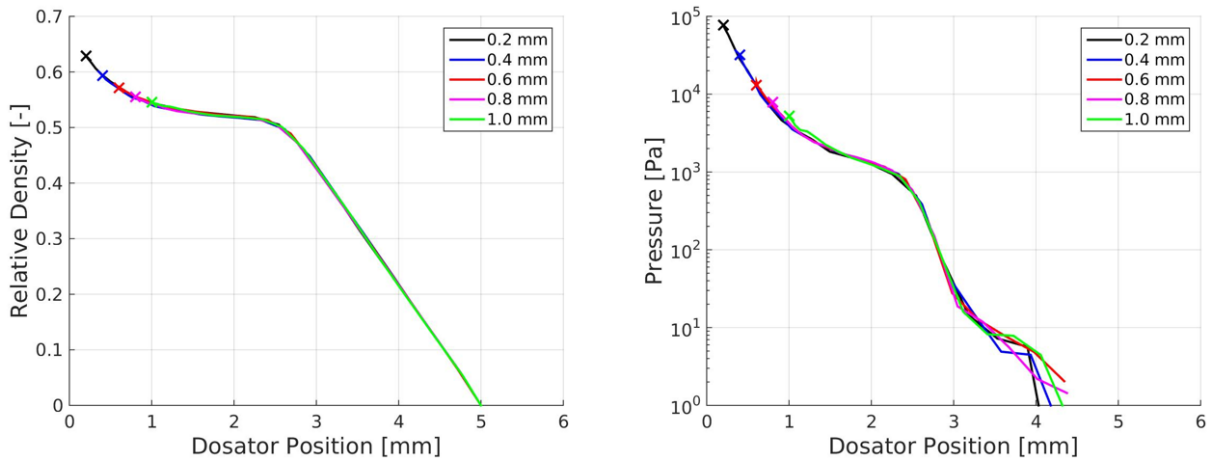


Fig. 15: Results for different values of the gap width. The end point of each run is marked with an 'x'.

4.4 Dosator geometry

4.4.1 Dosator diameter

For the investigation of the impact of the dosator diameter on the capsule filling process, dosator nozzles with diameters between 1.9 and 3.4 mm were used. Obviously a bigger diameter leads to more dosed mass due to the higher volume of the dosator. But the results in Fig. 16 show that also the powder density inside the dosator increases and the powder is more compacted. If volumetric filling would occur (doubled dosator volume leads to doubled mass) as suggested by (Faulhammer et al., 2014a), the relative density would remain constant. (Stranzinger et al., 2017) already observed in their experiments that volumetric filling can't be assumed for the dosator process. The slope in the first stage is higher for bigger dosator diameters, although the pressure is approximately the same for all cases. This implies that more powder is filled into the dosator with the same stress acting on the particles. This effect can be explained with less bridging effects for bigger diameters. On the other hand more compression is needed for larger dosator nozzles to retain a stable plug.

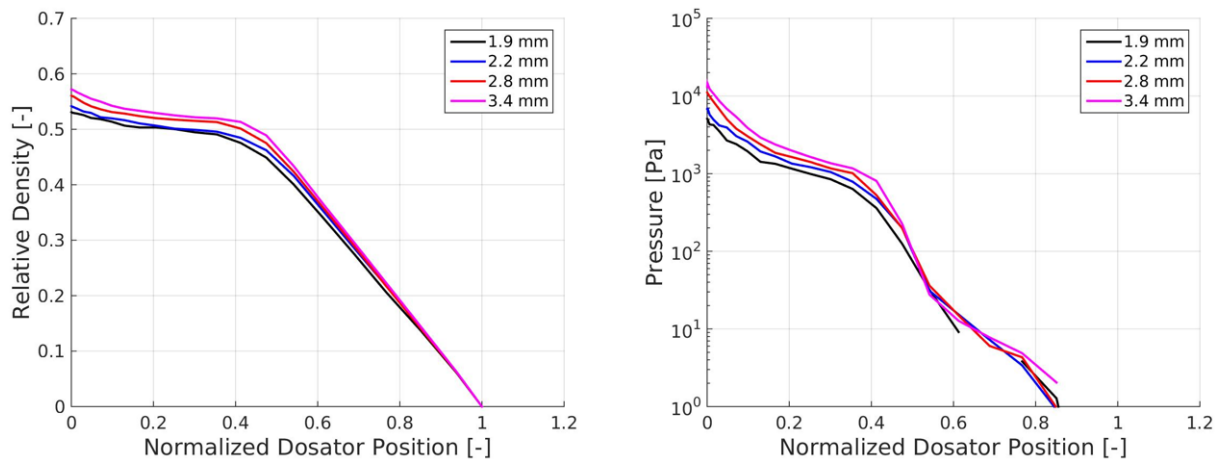


Fig. 16: Results of the simulations for different dosator diameters.

4.4.2 Chamber length

Changing the chamber length has an indirect proportional effect on the precompression ratio. The same precompression ratios as in section 4.2 are used, leading to chamber lengths between 1 and 3.333 mm. Since the volumetric filling stage ends when the whole dosator chamber has dipped into the bed, its duration is proportionally longer for lower precompression ratios (longer dosator chamber). Fig. 17 shows that the impact on the relative density is rather small, and in contrast to the dosator diameter, lower values cause higher densities. Therefore a higher precompression ratio leads to more mass, which is in accordance with the results of the bed height variations although it plays a minor role. However, the impact of the chamber length seems to be underestimated in the simulation, as the experiments of (Faulhammer et al., 2014a) and (Stranzinger et al., 2017) indicate a significantly higher influence on the density. A possible solution for this problem could be higher wall friction parameters.

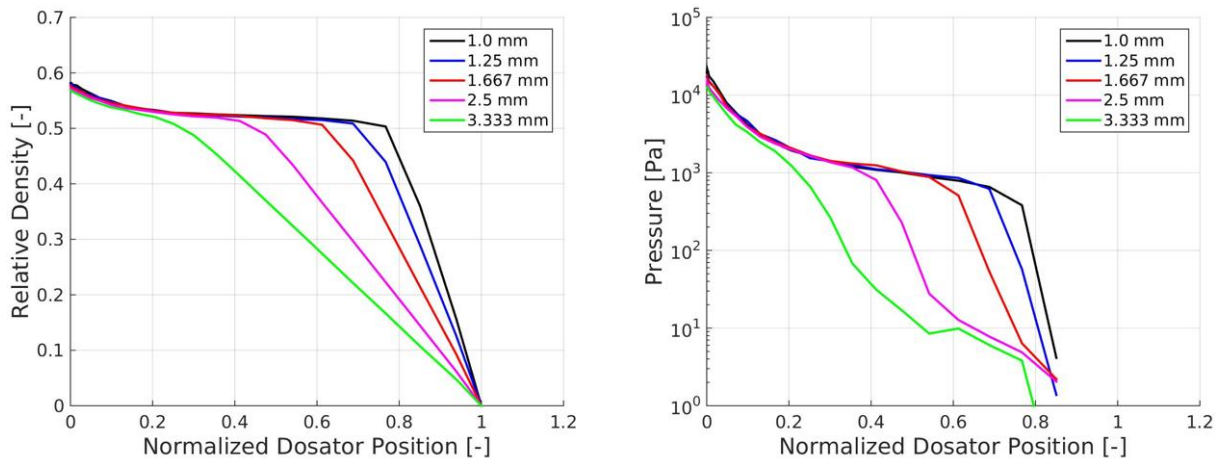


Fig. 17: Relative density and pressure for various chamber lengths. The chamber length was chosen in a way that the precompression ratios are equal to the ones in section 4.2.

4.4.3 Constant precompression ratio

In the simulations shown in Fig. 18 different powder bed heights from 3.75 to 10 mm were used. The chamber length was adjusted in a way that the precompression ratio stayed at a constant value of 2, i.e. the chamber length was half the size of the powder bed height (1.875 to 5 mm). The density remains nearly the same for every run, a variation between the highest and lowest value of less than 0.6% was observed. Also the pressure converges towards the same value at the end of the dipping step. Due to the constant density, it could be assumed that the precompression ratio can be used for scaling the process, but (Stranzinger et al., 2017) assert that this is not possible. The results of the simulation are probably affected by the underestimation of the chamber length effects.

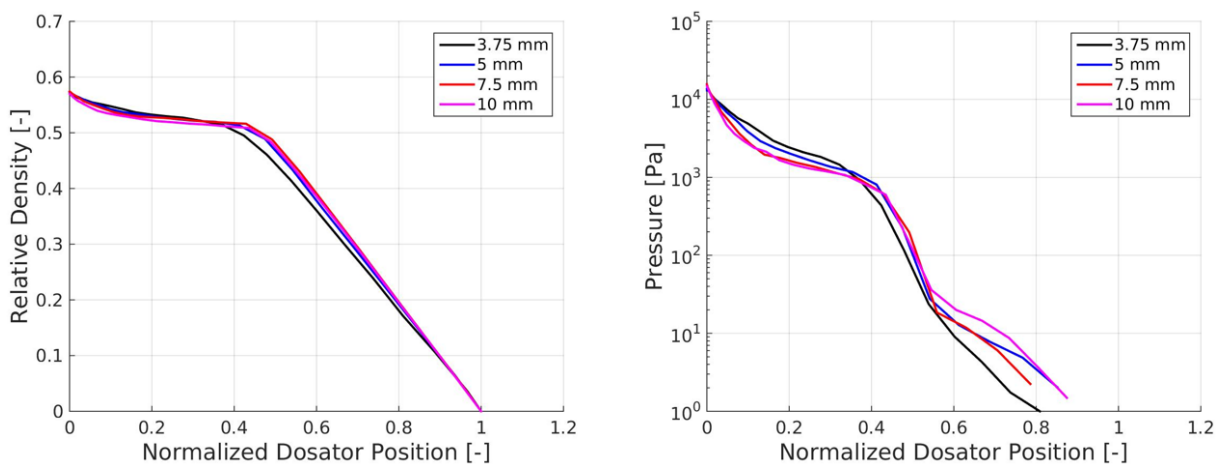


Fig. 18: Different powder bed heights and chamber length with a precompression ratio of 2 lead to similar results. In the legend the powder bed height is stated.

4.4.4 Constant diameter to chamber length ratio

In the following simulations the diameter was varied between 1.9 and 3.4 mm and the chamber length ranges between 1.4 and 2.5 mm, to keep the ratio of diameter to chamber length constant at 1.36. The results (Fig. 19) are in accordance with the ones of section 4.4.1. Since bigger diameters cause less bridging effects and lead to higher densities. Due to the lower precompression ratio for bigger diameters, stage one gets proportionally longer. The compression stage starts roughly at the same point for all cases.

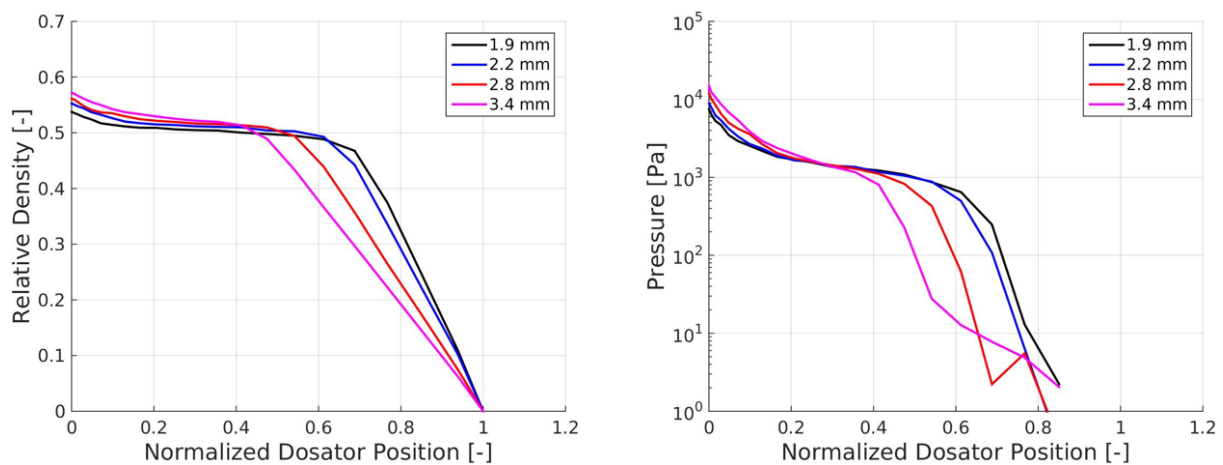


Fig. 19: Results for a constant diameter to chamber length ratio of 1.36. In the legend the diameter is given.

4.4.5 Constant dosator volume

In Fig. 20 the results for different dosator geometries with constant volume are pictured. The diameters range from 1.9 to 3.4 mm, the chamber length is in between 2.5 and 8 mm. A powder bed height of 10 mm was chosen instead of the standard value of 5 mm to theoretically be able to fill all dosators. Evidently the dosator process does not exhibit volumetric filling, otherwise the results of each run would be identical. There are enormous differences especially for smaller diameters. Fig. 21 shows that the dosator isn't filled properly for a diameter of 1.9 mm. The 2.2 mm dosator still has many voids, which disappear for larger diameters. The pressure profile doesn't indicate an end of the first stage for the two smallest diameters. For these dosators at some point during dosing the powder gets pushed aside instead of being filled into the dosator nozzle.

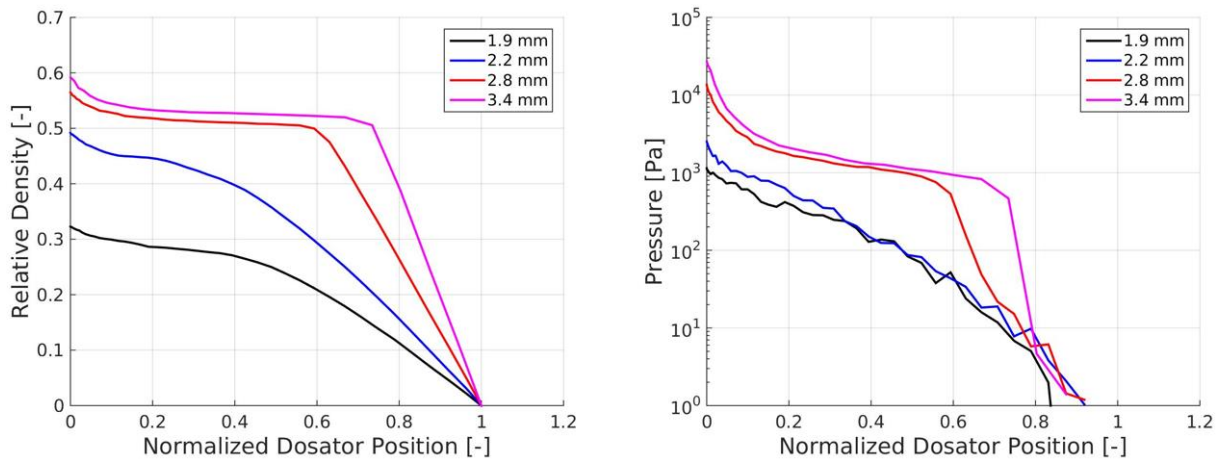


Fig. 20: Simulations with constant volume, but different diameters and chamber lengths confirm that the dosator process is not volumetric.

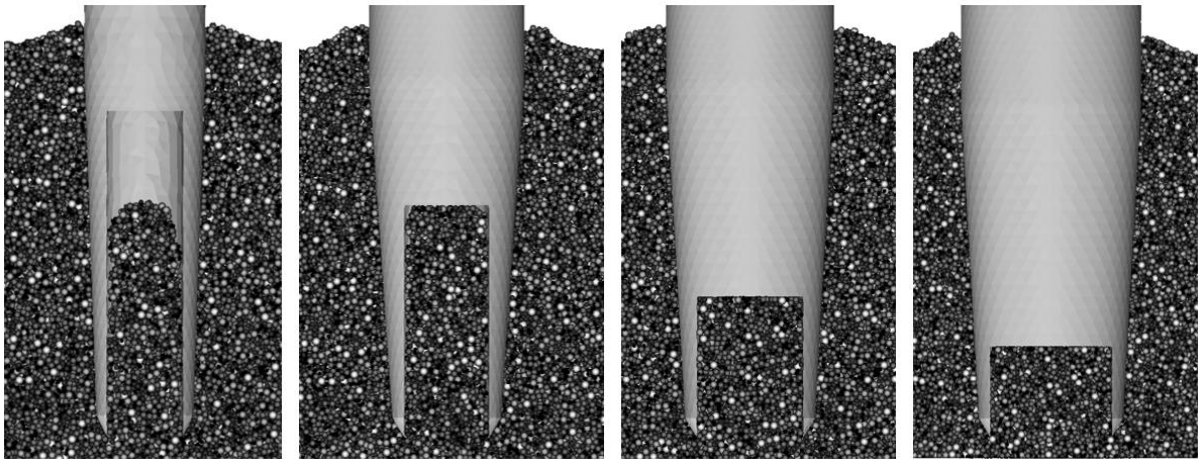


Fig. 21: Dosing with constant volume, the dosator diameter is increased from left (1.9 mm) to right (3.4 mm). With long and thin dosator chambers the powder cannot be dosed satisfactorily.

4.5 Bulk density

The influence of the initial settling velocity on the density of the powder bulk was discussed earlier. Now this influence is used for the investigation of the effect of varying bulk densities for constant contact properties. In Fig. 22 the results for settling velocities between 0.6 and 1.0 m/s are shown, giving bulk densities between 790 and 832 kg/m³. As expected, a higher bulk density leads to an increase in dosed mass. Due to the denser bed more mass is filled into the dosator during the first stage of filling. The pressure also rises with higher bulk density. The variations of the dosed mass in the simulations are rather small, since a comparable small increase in bulk density of 5% results in less than 1.5% increase in mass. The density variation in the real process may be bigger and therefore also the variations of dosed mass may be more important. In a real process the dosator compacts the bed with every dipping step, and the dosed powder has to be refilled. In this process it is difficult to

maintain a constant powder bed density especially for cohesive powders. Therefore steady state is hard to achieve and locally different bulk densities occur.

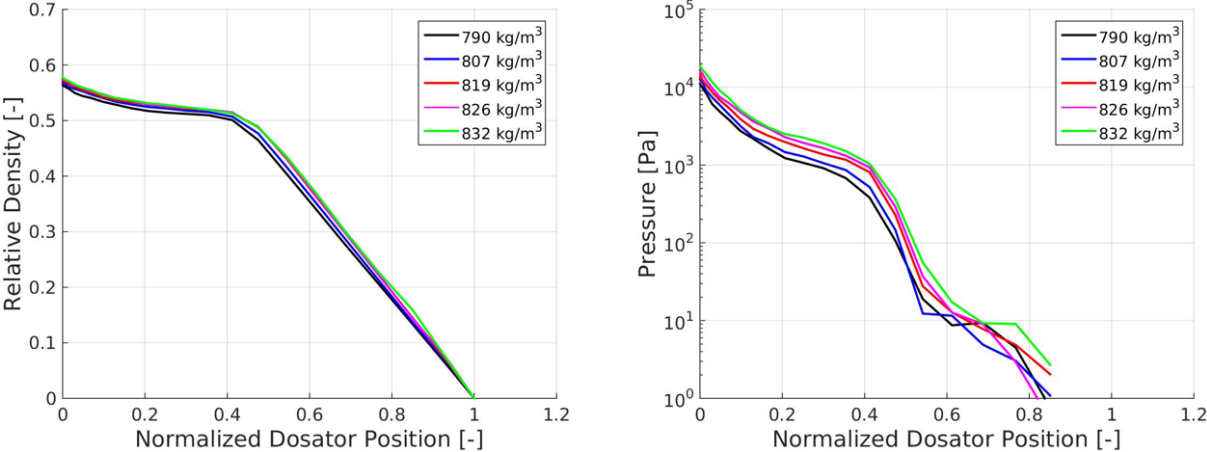


Fig. 22: Relative density and pressure inside the dosator for different bulk densities.

5 Conclusion and outlook

Critical process parameters of a dosator based capsule filling process were investigated in order to improve process understanding. To achieve this goal, numerical simulation based on the DEM approach was used. In contrast to experiments the simulation is able to observe relevant parameters during the dipping step. In this work the development of mass and pressure inside the dosator were recorded during dipping. Since contact models are needed in DEM for the calculation of the forces acting on particles, their ability to reproduce experiments has to be tested. For this purpose the Hertz model and the Luding model were investigated. First, a verification of the normal and tangential models of both contact models was performed successfully. Then the model parameters were determined in an iterative calibration procedure. In the validation step the results of twelve different settings were compared to experimental results. In opposition to the Hertz model, satisfactory outputs were obtained with the Luding model, which therefore was used for the process evaluation.

Machine speed doesn't have a big impact on capsule fill weight for the used material. However, increasing machine vibrations at higher dosing speeds were not considered. They could affect the fill weight due to powder densification, if other materials are used. A significant impact of the powder bed height was recorded, which is in accordance with literature. It can be expected that the effect increases for more cohesive powders since compressibility increases. The gap width between the lowest point of the dosator and the container bottom is a very sensitive parameter, since it determines the compression of the powder. Little variations lead to a significant change in capsule fill weight and therefore a constant gap width is essential for low fill weight variabilities. Furthermore the plug formation is affected, as a small gap causes high compression of the powder in the nozzle. The highly compressed powder could lead to problems during plug ejection. If the gap is chosen too high, no sufficient plug formation may happen at all, and in the worst case powder retention is not possible. Several different dosator geometries were investigated. Due to the different dosator volumes, the relative density inside the dosator was compared instead of the dosed mass, in order to get comparable results. The relative density increases for larger dosator diameters, since bridging effects are of less relevance. In contrast to literature, a significant influence of the dosator chamber length was not observed. One reason may be the non-adequate representation of the particle-wall contacts since the same model parameters were used as for particle-particle contacts. Only small deviations of the relative density were observed in the study of constant precompression ratio for variable powder bed heights and variable chamber lengths. Here also the insufficient modelled wall friction could be the reason for the variations compared to the experiments. The simulations

with constant diameter to chamber length ratio and constant dosator volume both showed that larger diameters lead to more densified plugs. No satisfactory filling was possible for very thin and long dosators. The results for varying the dosator geometry prove that volumetric filling is generally not obtained. Finally the impact of the bulk density of the powder bed was investigated. Powder beds with a higher bulk density lead to a higher capsule fill weight.

Although reasonable results were obtained, several improvements could be made regarding the modeling of the dosator process. First of all adjusting the wall parameters is necessary to achieve a more realistic representation of the filling behavior for a variation of the chamber length. The tangential part of the Luding model should be modified in a way that dynamic friction is active until the spring force is smaller than the dynamic friction force. Furthermore the introduction of a rolling friction model could be considered for particle shape correction. According to literature of dosator experiments (Faulhammer et al., 2014b; Stranzinger et al., 2017), it takes several minutes (more than 15 minutes for unfavorable process settings) until a steady state process is achieved due to variations in the powder bed when the dosator dips into it. Also the created holes have to be filled again. Therefore it may be advantageous to simulate repeated dosing. Another improvement could be the addition of a moveable piston inside the dosator, so that plug compression and ejection can be investigated. Moreover, a calibration of the contact model with different experiments than the dosator experiment is desirable. When the powder is calibrated successfully with several different processes, a quantitative analysis for every validated powder is possible.

6 Nomenclature

Abbreviations		Greek symbols	
CMA	Critical material attributes	γ	Damping coefficient
CPP	Critical process parameters	δ	Overlap
CQA	Critical quality attributes	θ	Phase shift
DEM	Discrete element method	μ	Friction coefficient
DoE	Design of experiments	ν	Poisson ratio
OFAT	One factor at a time	ρ	Density
		ϕ	Plasticity depth
		ω	Angular velocity
Symbols		Subscripts	
cl	Dosator chamber length	n	normal
d	Dosator diameter	t	tangential
e	Coefficient of restitution	eff	effective
F	Force	max	maximum
f	Factor for tangential parameters	hys	hysteresis
G	Shear modulus	c	cohesion
h	Powder bed height	k	stiffness
k	Stiffness	γ	damping
\hat{k}	Maximum stiffness	e	end
m	Mass	rel	relative
n	Machine speed	set	settling
R	Particle radius	0	pull off
Δt	Time step	1	particle 1, loading
v	Velocity	2	particle 2, unloading
\hat{v}	Maximum velocity		
\bar{v}	Mean velocity		
x	Particle position		
Y	Young's modulus		
z	Dosator position		

7 List of tables

Table 1: Parameters of the velocity profile for different machine speeds, powder bed heights and gap widths.....	11
Table 2: Model parameters for the Hertz model determined with the Bulk Calibration Approach.....	21
Table 3: Model parameters for the Luding model determined with the Bulk Calibration Approach.....	22
Table 4: Results of the validation runs for both contact models. The Luding contact model shows better agreement with the experimental data obtained from (Faulhammer et al., 2014a).....	22

8 List of figures

Fig. 1: Principle of the capsule filling process via the dosator method (Hoag, 2016).....	2
Fig. 2: The three steps of dosator filling: (i) volumetric filling step, (ii) intermediate step and (iii) compression step (Loidolt et al., 2017).	3
Fig. 3: (a) Collision of two spheres generates an overlap δ_n . (b) Spring-dashpot model in normal and tangential direction, connected via the friction coefficient μ	6
Fig. 4: Normal force hysteresis of the Luding contact model (modified from Luding, 2008).	9
Fig. 5: Cross section of the geometrical setup. Small particles are black, large particles are white.	10
Fig. 6: Verification setup for the (a) normal model and (b) tangential model.....	13
Fig. 7: Contact force of (a) a single particle-particle contact and (b) a particle-wall contact with and without damping force for the Hertz normal model.....	14
Fig. 8: Tangential force and particle velocity for the Hertz tangential model.	15
Fig. 9: Contact force of a single particle-particle contact (a) and a particle-wall contact (b) with and without damping force for the Hertz normal model.	16
Fig. 10: Verification of the Luding tangential model.....	17
Fig. 11: Particle size distribution	20
Fig. 12: Powder plug inside the dosator after the dipping step.....	24
Fig. 13: Relative density and pressure inside the dosator for different machine speeds.	26
Fig. 14: Relative density for different powder bed heights over the normalized dosator position (top left) and the absolute position (top right), as well as the pressure inside the dosator over the normalized dosator position (bottom left) and the absolute position (bottom right).	27
Fig. 15: Results for different values of the gap width. The end point of each run is marked with an 'x'.....	28
Fig. 16: Results of the simulations for different dosator diameters.	29
Fig. 17: Relative density and pressure for various chamber lengths. The chamber length was chosen in a way that the precompression ratios are equal to the ones in section 4.2.....	30
Fig. 18: Different powder bed heights and chamber length with a precompression ratio of 2 lead to similar results. In the legend the powder bed height is stated.....	30
Fig. 19: Results for a constant diameter to chamber length ratio of 1.36. In the legend the diameter is given.	31
Fig. 20: Simulations with constant volume, but different diameters and chamber lengths confirm that the dosator process is not volumetric.	32

Fig. 21: Dosing with constant volume, the dosator diameter is increased from left (1.9 mm) to right (3.4 mm). With long and thin dosator chambers the powder cannot be dosed satisfactorily. 32

Fig. 22: Relative density and pressure inside the dosator for different bulk densities. 33

9 References

- Asaf, Z., Rubinstein, D., Shmulevich, I., 2007. Determination of discrete element model parameters required for soil tillage. *Soil Tillage Res.* 92, 227–242. <https://doi.org/10.1016/j.still.2006.03.006>
- Coetzee, C.J., 2017. Review: Calibration of the discrete element method. *Powder Technol.* 310, 104–142. <https://doi.org/10.1016/j.powtec.2017.01.015>
- Cundall, P.A., Strack, O.D.L., 1979. Cundall_Strack_1979. *Geotechnique.* <https://doi.org/10.1680/geot.1979.29.1.47>
- Faulhammer, E., Fink, M., Llusà, M., Lawrence, S.M., Biserni, S., Calzolari, V., Khinast, J.G., 2014a. Low-dose capsule filling of inhalation products: critical material attributes and process parameters. *Int. J. Pharm.* 473, 617–626. <https://doi.org/10.1016/j.ijpharm.2014.07.050>
- Faulhammer, E., Llusà, M., Radeke, C., Scheibelhofer, O., Lawrence, S., Biserni, S., Calzolari, V., Khinast, J.G., 2014b. The effects of material attributes on capsule fill weight and weight variability in dosator nozzle machines. *Int. J. Pharm.* 471, 332–338. <https://doi.org/10.1016/j.ijpharm.2014.05.058>
- Fisher, R.A., 1936. The Design of Experiments. *Am. Math. Mon.* 43, 180. <https://doi.org/10.2307/2300364>
- Hertz, H., 1881. Über die Berührung fester elastischer Körper. *J. für die reine und Angew. Math.* 171, 156–171. <https://doi.org/10.1515/crll.1882.92.156>
- Hoag, S.W., 2016. Capsules dosage form: Formulation and manufacturing considerations, *Developing Solid Oral Dosage Forms: Pharmaceutical Theory and Practice: Second Edition.* Elsevier Inc. <https://doi.org/10.1016/B978-0-12-802447-8.00027-3>
- Johnstone, M.W., 2010. Calibration of DEM models for granular materials using bulk physical tests. The University of Edinburgh.
- Joliffe, I.G., Newton, J.M., Walters, J.K., 1980. Theoretical Considerations of the filling of pharmaceutical hard gelatine capsules 37, 189–195.
- Joliffe, I.G., Newton, J.M., 1982. An investigation of the relationship between particle size and compression during capsule filling with an instrumented mG2 simulator. *J. Pharm. Pharmacol.* 34, 415–419. <https://doi.org/10.1111/j.2042-7158.1982.tb04747.x>
- Jones, B.E., 2001. The filling of powders into two-piece hard capsules. *Int. J. Pharm.* 227, 5–26. [https://doi.org/10.1016/S0378-5173\(01\)00781-5](https://doi.org/10.1016/S0378-5173(01)00781-5)
- Khawam, A., Schultz, L., 2011. Modeling powder encapsulation in dosator-based machines: II. Experimental evaluation. *Int. J. Pharm.* 421, 210–219. <https://doi.org/10.1016/j.ijpharm.2011.09.027>
- Kleijnen, J.P.C., 1995. Verification and validation of simulation models. *Eur. J. Oper. Res.* 82, 145–162. <https://doi.org/10.1109/WSC.2000.899697>

- Kloss, C., 2016. LIGGGHTS(R)-PUBLIC Documentation, Version 3.X [WWW Document]. URL <http://www.cfdem.com/media/DEM/docu/Manual.html>
- Kloss, C., Goniva, C., Hager, A., Amberger, S., Pirker, S., 2012. Models , algorithms and validation for opensource DEM and CFD-DEM. *Pcfd* 12, 140–152. <https://doi.org/10.1504/PCFD.2012.047457>
- Llusa, M., Faulhammer, E., Biserni, S., Calzolari, V., Lawrence, S., Bresciani, M., Khinast, J., 2014. The effects of powder compressibility, speed of capsule filling and pre-compression on plug densification. *Int. J. Pharm.* 471, 182–188. <https://doi.org/10.1016/j.ijpharm.2014.04.073>
- Llusa, M., Faulhammer, E., Biserni, S., Calzolari, V., Lawrence, S., Bresciani, M., Khinasta, J., 2013. The effect of capsule-filling machine vibrations on average fill weight. *Int. J. Pharm.* 454, 381–387. <https://doi.org/10.1016/j.ijpharm.2013.07.029>
- Loidolt, P., Madlmeir, S., Khinast, J.G., 2017. Mechanistic Modeling of Capsule Filling Processes. *Int. J. Pharm.* 532, submitted. <https://doi.org/10.1016/j.ijpharm.2017.08.125>
- Lommen, S., Schott, D., Lodewijks, G., 2014. DEM speedup: Stiffness effects on behavior of bulk material. *Particuology* 12, 107–112. <https://doi.org/10.1016/j.partic.2013.03.006>
- Luding, S., 2008. Cohesive, frictional powders: Contact models for tension. *Granul. Matter* 10, 235–246. <https://doi.org/10.1007/s10035-008-0099-x>
- Macrae, J.C., Gray, W.A., 1961. Significance of the properties of materials in the packing of real spherical particles. *Br. J. Appl. Phys.* 12, 164–172. <https://doi.org/doi:10.1088/0508-3443/12/4/309>
- Malone, K.F., Xu, B.H., 2008. Determination of contact parameters for discrete element method simulations of granular systems. *Particuology*. <https://doi.org/10.1016/j.partic.2008.07.012>
- Marigo, M., Stitt, E.H., 2015. Discrete element method (DEM) for industrial applications: Comments on calibration and validation for the modelling of cylindrical pellets. *KONA Powder Part. J.* 32, 236–252. <https://doi.org/10.14356/kona.2015016>
- Pantaleev, S., Yordanova, S., Janda, A., Marigo, M., Ooi, J.Y., 2017. An experimentally validated DEM study of powder mixing in a paddle blade mixer. *Powder Technol.* 311, 287–302. <https://doi.org/10.1016/j.powtec.2016.12.053>
- Patel, R., Podczek, F., 1996. Investigation of the effect of type and source of microcrystalline cellulose on capsule filling. *Int. J. Pharm.* 128, 123–127. [https://doi.org/10.1016/0378-5173\(95\)04231-8](https://doi.org/10.1016/0378-5173(95)04231-8)
- Rackl, M., Hanley, K.J., 2017. A methodical calibration procedure for discrete element models. *Powder Technol.* 307, 73–83. <https://doi.org/10.1016/j.powtec.2016.11.048>
- Sargent, R.G., 2007. Verification and Validation of Simulation Models, in: *Proceedings of the 39th Conference on Winter Simulation: 40 Years! The Best Is Yet to Come.* pp. 124–137.
- Sastry, S., Nyshadham, J., Fix, J., 2000. Recent technological advances in oral drug delivery - a review. *Pharm. Sci. Technol. Today* 3, 138–145. [https://doi.org/10.1016/S1461-5347\(00\)00247-9](https://doi.org/10.1016/S1461-5347(00)00247-9)

- Shah, K., Augsburger, L.L., Small, L., Polli, G., 1983. Instrumentation of a dosing disc automatic capsule filling machine. *Pharm Tech* 7, 42–54.
- Small, L.E., Augsburger, L.L., 1977. Instrumentation of an Automatic Capsule-Filling Machine. *J. Pharm. Sci.* 66, 504–509. <https://doi.org/https://doi.org/10.1002/jps.2600660412>
- Stranzinger, S., Faulhammer, E., Calzolari, V., Biserni, S., Dreu, R., Šibanc, R., Paudel, A., Khinast, J.G., 2017. The effect of material attributes and process parameters on the powder bed uniformity during a low-dose dosator capsule filling process. *Int. J. Pharm.* 516, 9–20. <https://doi.org/10.1016/j.ijpharm.2016.11.010>
- Tan, S.B., Newton, J.M., 1990a. Minimum compression stress requirements for arching and powder retention within a dosator nozzle during capsule filling. *Int. J. Pharm.* 63, 275–280. [https://doi.org/https://doi.org/10.1016/0378-5173\(90\)90134-P](https://doi.org/https://doi.org/10.1016/0378-5173(90)90134-P)
- Tan, S.B., Newton, J.M., 1990b. Powder flowability as an indication of capsule filling performance. *Int. J. Pharm.* 61, 145–155. [https://doi.org/https://doi.org/10.1016/0378-5173\(90\)90053-7](https://doi.org/https://doi.org/10.1016/0378-5173(90)90053-7)
- Walker, D.M., 1966. An approximate theory for pressures and arching in hoppers. *Chem. Eng. Sci.* 21, 975–997. [https://doi.org/10.1016/0009-2509\(66\)85095-9](https://doi.org/10.1016/0009-2509(66)85095-9)
- Walters, J.K., 1977. A theoretical analysis of stresses in axially-symmetric hoppers and bunkers. *Chem. Eng. Sci.* 28, 779–789. [https://doi.org/10.1016/0009-2509\(77\)80012-2](https://doi.org/10.1016/0009-2509(77)80012-2)
- Wilkinson, S.K., Turnbull, S.A., Yan, Z., Stitt, E.H., Marigo, M., 2017. A parametric evaluation of powder flowability using a Freeman rheometer through statistical and sensitivity analysis: A discrete element method (DEM) study. *Comput. Chem. Eng.* 97, 161–174. <https://doi.org/10.1016/j.compchemeng.2016.11.034>